Bulletin of Volcanology (2019) 81: 62
https://doi.org/10.1007/s00445-019-1322-9

RESEARCH ARTICLE

Overview, chronology, and impacts of the 2016–2017 eruption of Bogoslof volcano, Alaska

Michelle Coombs[1] · Kristi Wallace[1] · Cheryl Cameron[2] · John Lyons[1] · Aaron Wech[1] · Kim Angeli[3] · Peter Cervelli[4]

Received: 10 April 2019 / Accepted: 2 September 2019 / Published online: 5 November 2019

Abstract

The 2016–2017 eruption of Bogoslof volcano, a back-arc shallow submarine volcano in Alaska's Aleutian arc, began in December 2016 and included 70 explosive events and at least two episodes of subaerial dome building. Because the volcano had no local monitoring stations during the eruption, a combination of distant seismic stations, regional infrasound sensors, lightning detection, a variety of satellite data and observer reports, and a field visit in 2018, were used to recreate the events that occurred during the nine-month eruption. Following precursory seismicity that started in September 2016, the eruption began in December 2016 with a series of explosive events that persisted through mid-March 2017. After a 6-week hiatus, activity resumed on May 17 and lasted through the end of August 2017 and consisted of additional explosions and two short-lived subaerial lava domes that formed in June and August. For most of the eruption, Bogoslof's vent was submerged in shallow seawater, though during several of the longer events a subaerial edifice grew, and the vent migrated above sea level resulting in more ash-rich volcanic clouds. Eruptive products, geophysical signals, and eruptive style are all broadly consistent with vulcanian activity where slow magma ascent led to repetitive dome or plug formation, overpressurization in the upper conduit, and sudden release during short-lived explosions. Infiltration of seawater may have prohibited large domes from forming especially in the first half of the eruption when explosions were closely spaced in time. The largest four explosions in the sequence occurred after inter-event times of 10 days or more. Three events produced ashfall on nearby communities and mariners east and south of Bogoslof and the eruption resulted in dozens of flight cancelations and flight diversions around the volcano and its ash clouds.

Keywords Surtseyan · Eruption response · Island volcano · Lava dome

This paper constitutes part of a topical collection:
The 2016-17 shallow submarine eruption of Bogoslof volcano, Alaska

Editorial responsibility: D. Fee

Electronic supplementary material The online version of this article (https://doi.org/10.1007/s00445-019-1322-9) contains supplementary material, which is available to authorized users.

✉ Michelle Coombs
mcoombs@usgs.gov

[1] U.S. Geological Survey, Alaska Volcano Observatory, Volcano Science Center, Anchorage, AK, USA

[2] Alaska Division of Geological & Geophysical Surveys, Alaska Volcano Observatory, Fairbanks, AK, USA

[3] U.S. Geological Survey, National Civil Applications Center, Reston, VA, USA

[4] U.S. Geological Survey, Volcano Science Center, Anchorage, AK, USA

Introduction

In 2016, Bogoslof volcano, a small back-arc volcano in the eastern Aleutian volcanic arc (Fig. 1), began a 9-month-long eruptive sequence that included at least 70 explosions, each minutes to hundreds of minutes long that sent ash clouds as high as 13 km above sea level (Fig. 2; Table 1). The eruption also produced at least two subaerial lava domes and caused dramatic morphologic changes to small Bogoslof Island, the subaerial tip of this mostly submerged volcano. Because Bogoslof Island is remote and uninhabited, like many Alaska volcanoes, the main hazards associated with the 2016–2017 eruption were from airborne ash with potential impacts to regional and trans-Pacific aircraft, and ashfall on moderately distant population centers and ships navigating along local routes. Communities at risk included Dutch Harbor/Unalaska, the most populous in the Aleutian Islands and the largest commercial fishing seaport in North America.

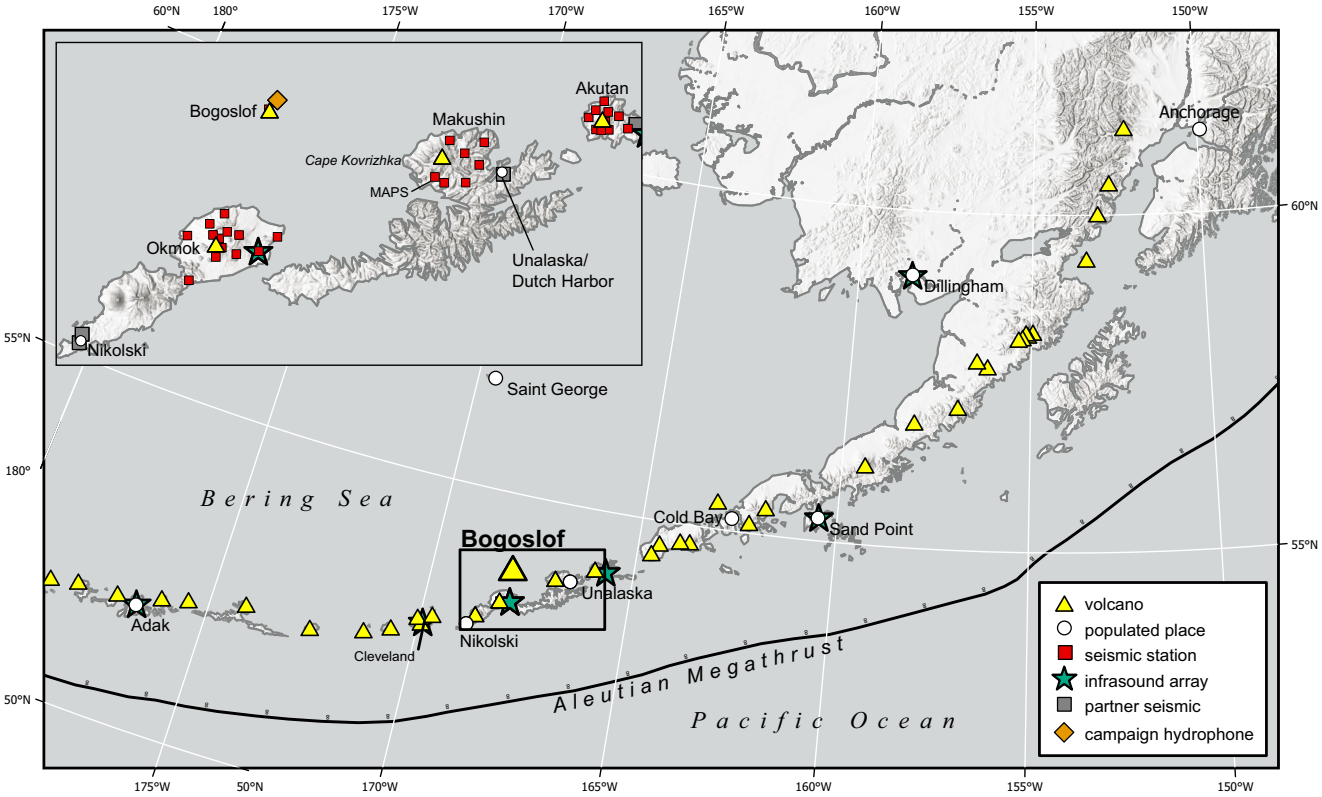

Fig. 1 Map of Alaska's Aleutian volcanic arc, showing historically active volcanoes as yellow triangles and notable communities as white circles. The inset map shows Bogoslof Island and nearby islands with volcano-monitoring equipment used during the 2016–2017 eruption

Eruptive sequences such as this one provide opportunities to study directly eruptive and magmatic processes, to improve monitoring techniques, and to apply the knowledge gained to future eruptions of this and analogous volcanoes. The 2016–2017 eruption of Bogoslof, which lacked a local geophysical network, was monitored by an array of techniques, which, in tandem with operational tools such as automated alarms (Tepp 2018), allowed the Alaska Volcano Observatory (AVO) to issue rapid warnings of hazards to surrounding communities, mariners, and aviators (Coombs et al. 2018).

Many of the same data streams that were used to provide real-time forecasting and detection during the eruption have now yielded insights into eruptive processes. Despite the eruption's remote nature, it is one of the only shallow submarine, Surtseyan-style eruptions monitored with modern geophysical and remote-sensing techniques. To our knowledge, other such examples are rare but include the 2009 eruption of Hunga Ha'apai-Hunga Tonga, which was monitored by hydrophone array (Bohnenstiehl et al. 2013) and remote sensing (Vaughan and Webley 2010). At Bogoslof, seismic data

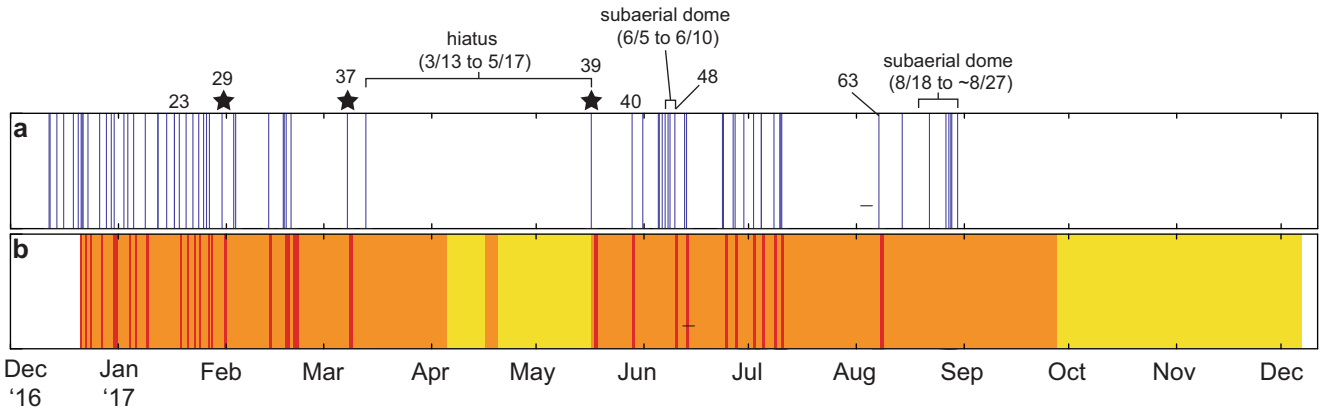

Fig. 2 Timeline of 2016–2017 Bogoslof eruption. **a** Explosive events are shown as vertical blue lines. **b** Aviation color code (no color = unassigned). Periods of subaerial dome growth and an eruptive hiatus are indicated by brackets, stars indicate explosive events that produced reported ashfall on land or mariners, and notable events as described in text are labeled

Table 1 Eruption parameters for numbered explosive events during the 2016–2017 eruption of Bogoslof volcano, Alaska

Event #[1]	Date (mm/dd/yy; UTC)	Eruption onset time (UTC)[2]	Event duration (with pauses; min)[3]	Infrasound duration (min)[4]	Seismic duration (min)[5]	# Seismic pulses	Max cloud height (km asl)[6]	Lightning strokes7	SO_2 cloud mass (Kt)[8]
Explosive phase I: rapid explosive events, common precursors (December 12, 2016–March 13, 2017)									
1	12-12-2016	12:40	220	7	nd	nd	nd	0	nd
2	12-12-2016	17:44	161	125	nd	nd	nd	0	nd
3	12-14-2016	22:10	nd	nd	51	8	2.6	0	nd
4	12-16-2016	18:39	6	1.5	35	2	6.1	41	0.8
5	12-19-2016	15:14	80	nd	94	3	nd	35	1.5
6	12-21-2016	0:38	47	nd	31	1	5	0	1.6
7	12-22-2016	1:22	20.5	9.5	4	1	8.7	114	4.1
8	12-22-2016	11:41	2	nd	nd	nd	nd	0	nd
9	12-23-2016	18:33	10	nd	nd	nd	nd	18	nd
10	12-26-2016	23:22	102	nd	60	2	8.5	59	1.5
11	12-29-2016	3:29	6	nd	45	1	nd	0	nd
12	12-30-2016	8:35	26	nd	36	1	5.1	0	nd
13	12-31-2016	7:33	45	nd	3	1	nd	56	3.2
14	1-2-2017	22:56	11	nd	11	1	nd	0	nd
15	1-4-2017	6:19	17	0.5	6	1	8.7	154	0.1
16	1-5-2017	22:30	19	4.5	6	1	11.8	41	0.2
17	1-9-2017	7:26	50	39.5	51	1	9.4	157	nd
18	1-12-2017	20:23	nd	nd	6	1	3.7	0	nd
19	1-12-2017	21:31	nd	nd	7	2	3.4	0	nd
20	1-15-2017	6:40	76	3	104	10	nd	5	*0.1*
21	1-17-2017	14:30	37	nd	54	1	3.4	0	*0.1*
22	1-17-2017	16:40	29	nd	31	1	2.6	0	–
23	1-18-2017	22:19	80	nd	62	7	8.5	14	1.9
24	1-20-2017	22:18	9	1	58	6	7.5	2	0.2
25	1-22-2017	23:00	5	nd	nd	nd	6.6	30	0.2
26	1-24-2017	13:51	15	2.5	58	2	7	68	0.5
27	1-26-2017	15:49	3	nd	4	3	5.5	24	0.6
28	1-27-2017	17:25	10	8.5	19	4	6.4 or 9.8	2	0.2
29	1-31-2017	5:18	409	117.5	19	11	5.9	190	3.6
30	2-3-2017	14:00	7	nd	28	2	nd	0	nd
31	2-4-2017	1:50	60	nd	55	2	4.6	0	nd
32	2-13-2017	16:24	nd	nd	92	4	5.9	0	0.1
33	2-17-2017	19:05	55	7	87	6	5.9	91	0.5
34	2-18-2017	0:34	13	nd	7	2	6.5	0	*0.7*
35	2-18-2017	14:00	4	nd	3	1	8.6	92	*1.4*
36	2-20-2017	2:08	40	18	10	5	6.1	20	0.7
37	3-8-2017	7:37	200	163.5	154	4	10.6 or 13.4	1437	21.5
38	3-13-2017	11:31	10	1.5	9	1	4.1	0	nd
Phase II: renewed explosive activity and dome building (May 17–August 30, 2017)									
39	5-17-2017	6:29	110	66.5	71	3	10	647	9.4
40	5-28-2017	22:16	46	24.5	49	1	10.1	719	7.7
41	6-1-2017	2:44	5	nd	5	1	7.3	0	nd
42	6-5-2017	15:50	1.5	0.5	1	1	nd	0	nd
43	6-5-2017	20:29	nd	nd	38	2	nd	0	nd
Dome observed (June 5, 2017)									
44	6-6-2017	13:59	2.5	1	1	1	nd	0	nd

Table 1 (continued)

Event #[1]	Date (mm/dd/yy; UTC)	Eruption onset time (UTC)[2]	Event duration (with pauses; min)[3]	Infrasound duration (min)[4]	Seismic duration (min)[5]	# Seismic pulses	Max cloud height (km asl)[6]	Lightning strokes7	SO_2 cloud mass (Kt)[8]
45	6-7-2017	14:28	5	3.5	1	1	1.5	0	nd
46	6-8-2017	5:28	1.5	nd	1	1	nd	0	nd
47	6-9-2017	0:58	4	0.5	2	1	3.2	0	nd
48	6-10-2017	9:58	300	83.5	25	6	9.5	31	1.6
49	6-13-2017	1:44	170	42	60	4	3.8	1	0.8
50	6-13-2017	16:15	2	1.5	5	1	nd	0	nd
51	6-24-2017	0:49	7	5	10	1	11.9	9	nd
52	6-24-2017	3:19	323	10.5	42	9	nd	0	nd
53	6-27-2017	0:44	nd	nd	12	2	8.6	0	0.1
54	6-27-2017	11:17	nd	nd	13	1	8.1	5	nd
55	6-30-2017	1:34	5	2	21	1	3.8	0	nd
56	7-2-2017	20:47	9	1.5	12	1	7.9	0	0.1
57	7-5-2017	0:51	12	10	12	1	8.4	1	nd
58	7-5-2017	3:05	13	5.5	12	1	6.9	0	nd
59	7-8-2017	18:15	nd	nd	12	2	6.5	0	nd
60	7-10-2017	7:46	166	10	54	7	nd	0	nd
61	7-10-2017	17:59	7	6.5	8	1	nd	0	nd
62	7-11-2017	1:07	nd	nd	14	1	nd	0	nd
63	8-7-2017	18:21	120	10	209	12	10.8 or 12.7	117	5.8
64	8-14-2017	16:49	5	nd	7	2	nd		nd
Dome observed (August 18, 2017)									
65	8-22-2017	12:06	3.5	1.5	1	1	nd	0	nd
66	8-27-2017	0:28	6	4	2	1	9.2	1	1.2
67	8-27-2017	23:08	2	1.5	1	1	8.7	0	0.3
68	8-28-2017	11:22	2	1.5	4	2	nd	0	*0.2*
69	8-28-2017	19:17	5	nd	2	1	6.7	0	*0.1*
70	8-30-2017	12:30	59	nd	18	9	8.5	2	0.4

[1] Events (explosions) defined using seismicity, infrasound, satellite imagery, lightning, and observations

[2] Derived from re-analysis using a combination of seismic, infrasound, and lightning data

[3] Calculated from first to last infrasound detection, including pauses

[4] Total number of minutes that the OKIF array detected coherent infrasound using the parameters of Lyons et al. (2019b)

[5] Total number of minutes that seismic signal was above twice background lasting for more than 10 s. Lulls in activity of 90 s or less are considered a continuation of activity (Searcy and Power 2019)

[6] Derived from reanalysis of satellite data (Schneider et al. 2019)

[7] Within 50 km of Bogoslof as reported by Vaisala (Van Eaton et al. 2019)

[8] Calculated as the mean of IASI A and B derived masses for the overpass with the greatest confirmed SO_2 mass from a particular Bogoslof event within 1 day of eruption (Lopez et al. 2019)

nd, not detected; none, none reported

Expanded eruption chronology can be found in ESM 1 and ESM 2

provide insights into eruption precursors and co-eruptive tremor (Tepp and Haney 2019; Haney et al. 2019a; Searcy and Power 2019; Tepp et al. 2019) and magma ascent and recharge (Wech et al. 2018). Analysis of infrasound data from explosive activity (Lyons et al. 2019b) reveals critical information about eruptive activity, including transitions between subaerial and submarine eruption (Fee et al. 2019) and creation of giant bubbles during shallow submarine hydrovulcanian explosive events (Lyons et al. 2019a). Satellite imagery and lightning data combine to reveal the dynamics of ice-rich volcanic clouds (Schneider et al. 2019; Van Eaton et al. 2019). High-resolution satellite images allow detailed tracking of deposits and morphologic and volume changes (Waythomas et al. 2019a). Analysis of eruptive

products provides information about magma generation and ascent (Loewen et al. 2019) and geologic studies of the eruptive deposits shed light on eruptive processes (Waythomas et al. 2019b).

In this paper, we present a chronology of the eruptive sequence, summarized in Table 1, with the benefit of these additional insights—critical for a volcanic eruption that was poorly documented by direct observations. We also describe the hazards and impacts from the eruption and discuss implications for future shallow submarine volcanic activity.

Bogoslof volcano

Bogoslof Island sits north of the Aleutian volcanic arc, about 100 km west of Unalaska/Dutch Harbor (Fig. 1). It is the tip of a mostly submerged back-arc volcano that last erupted in 1992, one of at least eight previous historical eruptions documented at Bogoslof (Waythomas and Cameron 2018). The 1992 eruption lasted about 3 weeks, produced episodic ash emissions up to 8 km above sea level (asl), and ended with extrusion of a lava dome (McGimsey et al. 1995). Previous historical eruptions lasted months to years and were characterized by intermittent explosive and effusive activity (Waythomas and Cameron 2018). Erupted compositions range from basalt through trachyte (Loewen et al. 2019). Elevated abundances of incompatible elements in eruptive products are consistent with Bogoslof's position behind the arc front, leading to deeper magma generation and lower degrees of partial melting (Loewen et al. 2019).

Prior to the 2016–2017 eruption, the subaerial portion of Bogoslof volcano consisted of two small islands, Bogoslof Island and Fire Island (total area in 2018 about 1.7 km^2; Fig. 3a). The submarine edifice of Bogoslof has ~ 1700 m of relief, and the highest point on Bogoslof Island is about 100–150 m above sea level. Bogoslof Island, 1.4 km long by about 500 m wide, consisted of three lava masses erupted in historical times and connected by low areas of pyroclastic material (Waythomas et al. 2019b). Fire Island is a small lava mass about 850 m NNW of Bogoslof Island.

Methods and data streams used to characterize the eruption

Direct observations of eruptive activity were scant in 2016–2017. Pilot reports or other observer reports sometimes provided details of explosive events, including cloud height, dispersal patterns, and simple confirmation of activity (Fig. 4). Other photographs from passers-by documented the changing morphology of the island (Fig. 5). In August 2018, geologists visited the island for the first time after the eruption to document the stratigraphy and character of new deposits (Waythomas et al. 2019b) and collect samples (Loewen et al. 2019).

High-resolution satellite data (Fig. 6) were used periodically throughout the eruption to track changing morphology, deposits, and eruptive features and to make inferences about eruptive processes (Waythomas et al. 2019a). Synthetic aperture radar (SAR) images from Cosmo SkyMed (sub-meter resolution Spotlight mode) and Sentinel-1 (~10-m resolution) satellites were useful for verifying the timing of some events (Fig. 7).

Real-time or near-real-time data streams were used to detect and characterize explosive activity quickly during the eruption, though no one data type recorded all explosive events. Due to its small size and wilderness designation, Bogoslof was not monitored by a local, on-island geophysical network during the 2016–2017 eruption. Instead, AVO used seismic sensors from Okmok (~ 54 km) and Makushin (~ 72 km) volcanoes on neighboring Umnak and Unalaska Islands (Fig. 1) to monitor seismic activity during the eruption (Coombs et al. 2018). The lack of a local network meant that low-level tremor and smaller earthquakes went undetected; AVO located 244 earthquakes during the eruption with a magnitude detection threshold of 0.6 (Tepp et al. 2019). Distance to closest seismic stations, coupled with poor azimuthal coverage, meant that these hypocenters were poorly constrained (Tepp et al. 2019). Using a matched filter approach on data from station MAPS located on Unalaska Island, and the located events, Wech et al. (2018) constructed a catalog of 3199 earthquakes with a magnitude detection threshold of ~ 0.5. On May 22, 2017, 5 months into the eruption, a hydrophone was deployed low on Bogoslof's submarine flank and recorded data onsite until October 2 when it was retrieved. Much closer than any of the seismic instruments, it recorded smaller explosive events and some precursory seismicity that had otherwise gone undetected, though only available after retrieval (Tepp et al. 2019).

Multiple infrasound sensors or arrays along the Aleutian arc provided an important data source during the eruption (Coombs et al. 2018; Lyons et al. 2019a, 2019b; Schwaiger et al. 2019; Fig. 1). Explosion infrasound was recorded at all AVO arrays over the course of the Bogoslof eruption, including stations located more than 800 km from the volcano, though no single array detected all explosive activity (Lyons et al. 2019b). Seasonal stratospheric wind variations strongly affect more distant propagation, such as to Dillingham (Schwaiger et al. 2019; Fig. 1), but even the most proximal array at Okmok (OKIF; 59 km to the south) only detected about two-thirds of the events (Lyons et al. 2019b) due to a combination of wind noise and likely atmospheric variability that is not captured in infrasound propagation models (Schwaiger et al. 2019). When available, however, data from OKIF had lower latency (~ 3 min) than the more distant arrays and allowed for rapid confirmation of explosive activity.

Fig. 3 Photographs of Bogoslof island before and during the 2016–2017 eruption. Notable features are labeled in panel **a**; southern tip of pyroclastic wedge is indicated in both panels by star. Distance from Castle Rock to Fire Island is about 1.7 km, and distance from denuded 1926 and 1992 lava domes in panel **b** is about 350 m. View in both photos is roughly towards the northwest. **a** Photo from May 1994. Note carapace of breccia and debris around the 1992 dome, and the relatively flat-lying pyroclastic deposits east of Castle Rock. Photo by Chris Nye, AVO-ADGGS. **b** View of Bogoslof volcano on January 10, 2017. Note uplifted area east of Castle Rock, though this area is not steaming. Photo courtesy of Dan Leary

Many explosions from Bogoslof generated volcanic lightning that was detected by the World Wide Lightning Location Network (WWLLN) and Vaisala network (Coombs et al. 2018; Van Eaton et al. 2019). Whereas WWLLN data were available to AVO in real time, that network records only an estimated 10 % of total lightning (Van Eaton and references therein). In the following chronology, we provide stroke numbers from Vaisala (Table 1), which had a greater sensitivity (Van Eaton et al. 2019), though neither of these global networks had the sensitivity achieved by local mapping arrays (Behnke et al. 2013). In some instances, infrasound instruments also detected volcanic thunder, a previously undocumented phenomenon, in conjunction with lightning (Haney et al. 2018). Retrospective analysis of data from the Okmok infrasound array showed that lightning strokes were also recorded as electromagnetic glitches there (Haney et al. 2019b).

During clear weather, or when volcanic clouds rose above the meteorological cloud deck, near real-time data from Advanced Very High-Resolution Radiometer (AVHRR), Moderate Resolution Imaging Spectroradiometer (MODIS), Visible Infrared Imaging Radiometer Suite (VIIRS), Geostationary Operational Environmental Satellite (GOES)-15, and Himawari-8 satellites were used to determine whether a volcanic cloud had been generated and to track its dispersion (Coombs et al. 2018). Data from these satellites were also used to determine cloud-height estimates by comparing cloud-top temperature to the atmospheric temperature profile determined from the Global Forecast System data (Schneider et al. 2019). Clouds were visible for 48 of 70 events (69 %). Satellite imagery was also used to assess whether hot tephra or lava was present at the surface (Electronic Supplement). Lopez et al. (2019) quantified SO_2 masses released by many of the explosive events using data from the Infrared Atmospheric Sounding Interferometer (IASI) satellite sensor.

The chronology of the 2016–2017 eruption of Bogoslof volcano

The 2016–2017 eruption of Bogoslof lasted 9 months and encompassed activity similar to that seen previously at the volcano—intermittent, short-lived explosions and dome building. Our chronology focuses on explosions large enough to be observed and/or detected geophysically, two episodes of observed lava dome effusion, and major morphologic changes to the island.

Fig. 4 Photographs of eruption plumes from explosive events during the 2016–2017 eruption of Bogoslof volcano. All dates and times given in UTC. **a** White plume from event 3, captured by ESA Sentinel-2A satellite, December 14, 2016, at 22:29. **b** Eruption plume from event 6, taken at about 00:30 on December 21, 2016. The aircraft from which the photo was taken was about 32 km north of Bogoslof Island flying westbound at an altitude of about 11 km. Image courtesy of Paul Tuvman. **c** Plume from event 16, January 5, 2017. Photo courtesy of Trever Shaishnikoff. **d** Dark-gray plume (dashed box) from event 23 on January 18, 2017, as seen in image captured at 22:29 by a west-facing webcam in Dutch Harbor that is maintained by the Federal Aviation Administration. **e** Eruption cloud from event 36 on February 20, 2017, as seen from Unalaska Island. Photo taken from helicopter during fieldwork by AVO geologists at 02:22, approximately 14 min after the start of the eruption. **f** Worldview satellite image collected at 22:34 on May 28, 2017, showing the development of the eruption cloud from event 40. The eruption began about 18 min prior to this image and the cloud rose to an altitude 10.1 km asl. Image data provided under the Digital Globe NextView License

Explosions were typically identified by a combination of seismic and infrasound data and were assigned sequential numbers (Table 1, Fig. 8, and ESM 1)—event numbers are bolded at the first mention of each in the following text. Our catalog includes 70 numbered explosive events, but others were undoubtedly missed because they were below our detection threshold. Onset times are derived from a reanalysis of all geophysical data, and not a single source. All times are given in Universal Coordinated Time (UTC). Total event durations were determined using infrasound data and include the entire duration for each event, including some pauses between signals. The seismic durations of Searcy and Power (2019) were measured from when the signal exceeded twice background for more than 10 s. For some events, the seismic signal was pulsatory, and thus the seismic duration is shorter than the infrasound duration (Table 1). Other data streams shown in Table 1 and described below are from sources described above in the methods section. A more detailed, event-by-event version of the following chronology is presented in ESM 2.

Precursory phase (September to December 12, 2016)

Without a local seismic network, precursory seismicity was only recognized retrospectively. Wech et al. (2018) show that seismicity first occurred in September in the form of volcano-tectonic earthquakes, mostly on September 28–29 (swarm S1 of Tepp et al. 2019). Wech et al. (2018) interpret these events as likely caused by magmatic intrusion into the middle to upper crust. A smaller earthquake swarm occurred in early October, with sporadic earthquakes continuing until the eruption in December (Tepp et al. 2019).

Fig. 5 Photographs of Bogoslof Island during the 2016–2017 eruption. Notable features are marked as follows: Fire Island, F; Castle Rock, C; 1926–1927 lava dome, 26; 1992 lava dome, 92. **a** May 8, 2017, near the end of the ~ 6-week eruptive hiatus that lasted from March 13 to May 17. View is from the north, and Fire Island is in the foreground with steaming crater lagoon visible behind the 1992 and 1926–1927 lava domes. Photo by Max Kaufman, UAFGI/AVO, aboard USCG Cutter *Mellon*. **b** Bogoslof seen from Alaska Airlines flight from Adak to Anchorage on May 18, 2017, just after event 39. Photo by M. Kaufman. **c** Bogoslof seen from Alaska Airlines flight from Adak to Anchorage on June 22, 2017, between explosive events 50 and 51. Photo by Cyrus Read, USGS/AVO. **d** Views of Bogoslof volcano, looking northeast. Photo taken July 3, 2017, by John Farris, aboard the R/V *Tiglax*. This was taken between explosive events 56 and 57, and shows plume rising from the area of persistent steaming seen in 6b. Photo courtesy of the photographer and the US Fish and Wildlife Service. **e** Oblique airphoto taken on August 15, 2017, showing enclosed vent area with little water disruption in the area where the third lava dome would appear on August 18. Photo by Janet Schaefer, AVO-ADGGS. **f** Bogoslof volcano with a vigorous steam plume caused by interaction of the new, hot lava dome, just visible beyond the 1926–1927 lava dome, with seawater. This dome was likely destroyed on August 30 by the final explosive event of the eruption. Photo by Dave Withrow, NOAA, taken at about 21:00 on August 26, 2016, 24 nautical miles from Bogoslof

Phase 1 (December 12, 2016 to March 13, 2017)

From December 12 through March 13, explosions occurred at a mean rate of once every 58 h (2.4 days). Many of the explosions during this period were preceded by repeating earthquakes that accelerated into an explosion, characterized by increasing magnitude and becoming closer together in time, described by Wech et al. (2018) as "slow-clap" seismicity and also described in Tepp et al. (2019) and Tepp and Haney (2019). On the basis of *T*-phase character, Wech et al. (2018) interpret these as occurring in the shallow crust.

Events 1–5 (December 12–19, 2016)

Seismicity remained at fairly low levels in October and November. In early December, days before the first detected infrasound, earthquakes with weak *T*-phases again suggested mid- to shallow-crustal magma movement (Wech et al. 2018). On December 12, the first infrasound signal from Bogoslof marked the beginning of the eruption. The signal, later recognized as **event 1**, was accompanied by a weak seismic signal, but no cloud was observed in satellite images. Infrasound for **event 2**, later the same day, has a relatively high frequency index (FI; ratio of high-frequency to low-frequency infrasound),

Fig. 6 Select Worldview satellite images of Bogoslof from before, during, and after the 2016–2017 eruption. **a** March 19, 2015, over a year before eruption. **b** December 25, 2016. **c** January 11, 2017. **d** January 31, 2017. **e** February 12, 2017. **f** March 3, 2017. **g** March 11, 2017. **h** May 11, 2017. **i** June 12, 2017. **j** August 8, 2017. **k** August 13, 2017. **l** November 2, 2017. Worldview data provided under the Digital Globe NextView License

suggesting a subaerial vent (Fee et al. 2019). On December 14, AVO received an email report from St. George, 308 km north-northwest of Bogoslof, about intermittent sulfur smell, likely corresponding to activity at Bogoslof. A Sentinel-2 satellite image taken minutes after **event 3** on December 14 captured intense steaming from a subaerial vent and new

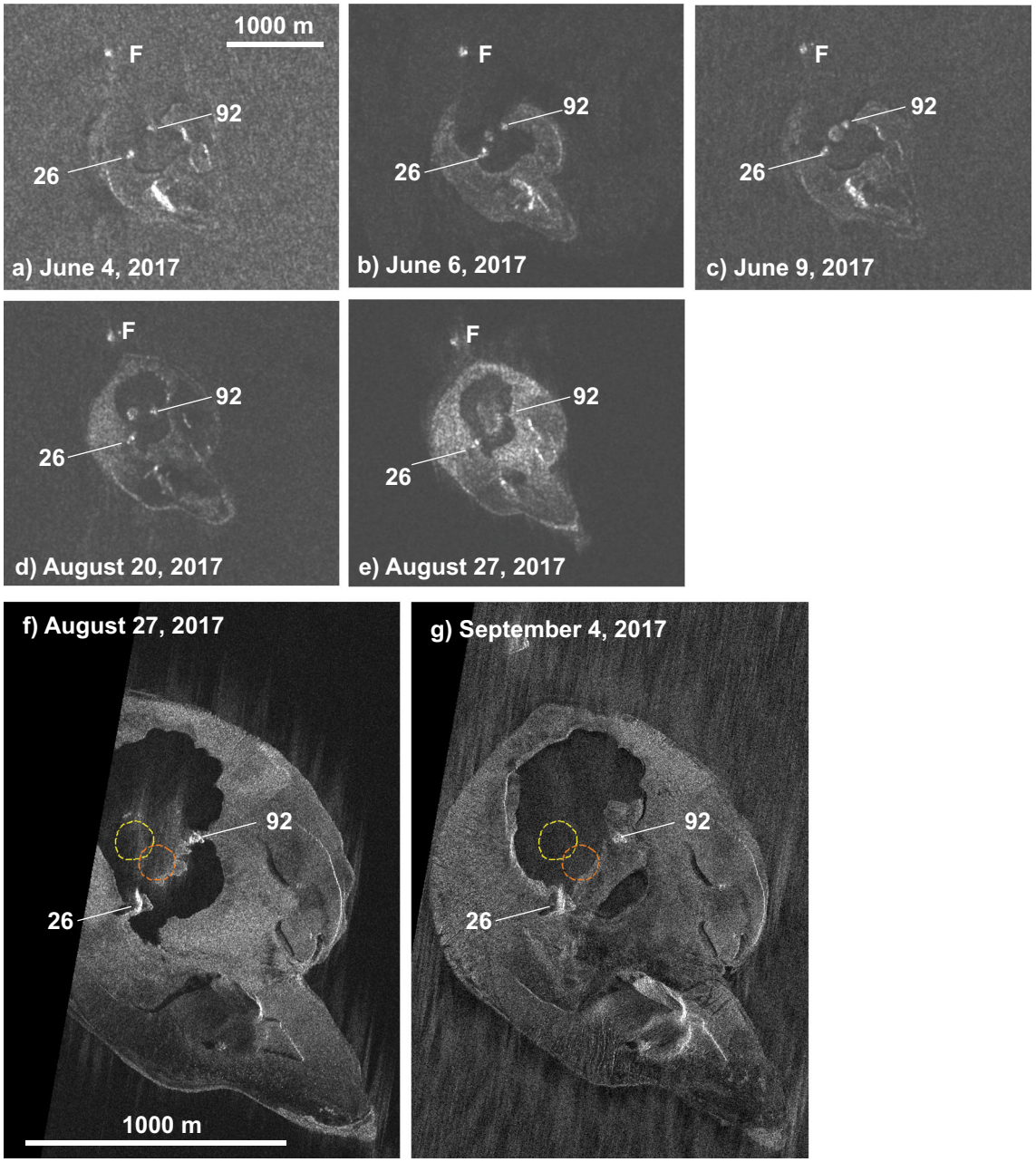

Fig. 7 Synthetic aperture radar images used to determine timing of dome growth and destruction in June and August 2017. **a** Sentinel-1B image from June 4, 2017, at 04:56 UTC, showing no dome in the crater lagoon. **b** Sentinel-1A image from June 6, 2017, at 17:21 UTC showing new dome. **c** Sentinel-1B image from June 9, 2017, at 05:04 UTC showing enlarged dome. **d** Sentinel-1B image from August 20, 2017, at 05:04 UTC. The dome is visible in the water-filled crater. **e** Sentinel-1B image from August 27, 2017, at 04:56 UTC. All or most of the dome is destroyed with some disruption to or deposition in the water-filled crater. **f** Cosmo SkyMed image from August 27, 2017, at 05:14 UTC. Similar features as Sentinel image from nearly the same time shown in (e.g., Cosmo SkyMed image from September 4, 2017, at 05:14 UTC). The August dome is no longer present. In last two images, location of June and August domes are shown in orange and yellow, respectively. Acknowledgements to: ASF DAAC 2017, contains modified Copernicus Sentinel data 2017, processed by ESA, for Sentinel data; Italian Space Agency for Cosmos SkyMed data

pyroclastic deposits on the island and suspended in the surrounding ocean (Fig. 4a). **Events 4 and 5** occurred on December 16 and 19. These first five explosions were not detected in real time, only after retrospective analysis of data streams. Thus, we have no direct observations of the character of these explosions.

Uplift (December 14–on: cryptodome emplacement)

Satellite imagery beginning December 14 shows that uplift of Bogoslof Island occurred and may have been associated with cryptodome emplacement. A Sentinel-2 satellite image from December 21 (Waythomas et al. 2019a) shows an

approximately 300-m long oval-shaped raised mass just north of Castle Rock (a remnant lava dome from the 1796–1804 eruptive period; see Fig. 3). This feature was not present in a Sentinel-2 image from December 14 (Waythomas et al. 2019a; their Fig. 5a). Preliminary analysis of DEMs generated by stereo satellite pairs shows that this feature continued to grow throughout the eruption (A. Diefenbach, written comm. 2019).

No elevated surface temperatures were seen in satellite monitoring checks at Bogoslof until January 19, and neither the uplifted block nor surrounding areas were visibly steaming in December or January in a way that would be consistent with lava effusion (Figs. 3 and 6). Samples of the material exposed along the steep, eastward face of the uplift (see Waythomas et al. 2019b) are trachyandesite lava with 58–60 wt% SiO_2 and are a different composition than the dominant juvenile basalt magma erupted in 2016–2017 (Loewen et al. 2019). Given the lack of thermal signature, as well as the composition of this feature, we suggest that this uplifted feature is likely the roof above a shallow cryptodome.

Events 6–22 (December 21–January 17: frequent, short explosions)

Several pilots observed a volcanic cloud in the vicinity of Bogoslof on December 21 (Fig. 4b), and were the first alert to AVO that Bogoslof had become active. A pilot later the same day reported seeing "a new land mass" in the island cluster. This event, **event 6**, began a period of activity that lasted a little less than a month, with explosive **events 6–22** occurring at a rate of about one every 40 h. They produced volcanic clouds of heights up to 11 km, with variable durations (2 to 102 min), and about half produced detected lightning (Table 1). Most (80 %) consisted of single seismic pulses.

Some of the only direct observations of activity occurred during **event 9** on December 23, when observers aboard a Coast Guard vessel in the area reported ash emissions, lightning, and the ejection of incandescent lava and fragmental material that lasted about an hour. The cloud from event 16 on January 5 rose to 11.8 km asl and was observed by numerous pilots and mariners (Fig. 4c).

A Worldview-3 image from December 25 (Fig. 6b) shows a bilobate submarine vent area and new pyroclastic deposits enlarging the island and beginning to enclose a vent lagoon. On December 29, data derived from US National Imagery Systems indicated a nearly complete ring of pyroclastic deposits around a more circular, submerged, ~450-m-across vent area. On January 10, passengers on a helicopter that flew from Dutch Harbor to Bogoslof took photographs and video of the island that showed discolored and roiling water in the crescent-shaped vent area, and the area of uplift from December (Fig. 3b). A Worldview-3 image from January 11 (Fig. 6c) shows continued growth of the island, and abundant meter-scale ballistics on the north and south ends of the island (Waythomas et al. 2019a, their Fig. 7).

Event 23 (January 18: first ash-rich cloud)

Satellite images, pilot reports, and ground-based photos show that **event 23** on January 18 was the first demonstrably ash-rich cloud of the eruption sequence. Previous explosions produced clouds that were white in color with almost no ash signal in satellite data (Schneider et al. 2019).

Prior to event 23, as with many other explosions on the first half of the eruption, seismic stations on neighboring islands picked up precursory seismicity in the form of repeating earthquakes that became more closely spaced in time during the runup to the explosion (Tepp et al. 2019). These lasted for about 11 h. Infrasound data show that the explosion itself lasted about 80 min and was pulsatory (Lyons et al. 2019b), with seven discrete bursts of strong seismicity (Searcy and Power 2019). Despite the event's duration, only modest lightning was produced (14 strokes; Van Eaton et al. 2019).

Pilots reports, visual satellite images, and the west-facing FAA web camera in Dutch Harbor (Fig. 4d) indicated that the explosion produced a dark-gray ash cloud. MODIS satellite images show the cloud rose as high as 8.5 km asl before drifting northeast over the Alaska Peninsula. An ash signal in the brightness-temperature-difference (BTD) satellite retrieval was seen along the leading cloud edge, suggesting that the cloud interior may have been opaque (Schneider et al. 2019). This event produced 1.9 kt of SO_2 and was the first since event 13 on December 31 to produce more than 0.2 kt SO_2 (Lopez et al. 2019).

>A mid-infrared MODIS satellite image collected minutes after the explosion showed a possible "recovery pixel." These occur when the sensor encounters a very hot object and saturates, suggesting lava or hot tephra must have been present above the water surface (D. Schneider, written comm. 2017). These were the first elevated surface temperatures detected by satellite imagery of the eruption. Clouds moved in to obscure the volcano soon after, with no additional views prior to January 20. Because event 23 was not detected on the Okmok infrasound array, we do not have infrasound FI analysis for this event, which for other events provides information on subaerial versus submarine venting (Fee et al. 2019).

Events 24–28 (January 20–27)

In the week following event 23, five explosions (**events 24–28**) occurred with an average repose time of 42 h between them (Table 1, Fig. 8). These events had total infrasound durations of 3–15 min, produced modest lightning, observable volcanic clouds, and each up to 0.6 kt of SO_2 (Table 1). None showed a clear ash signature in satellite data.

A Worldview-2 image acquired about 10 h after event 26 shows the island with a lagoon, open to the east, with two

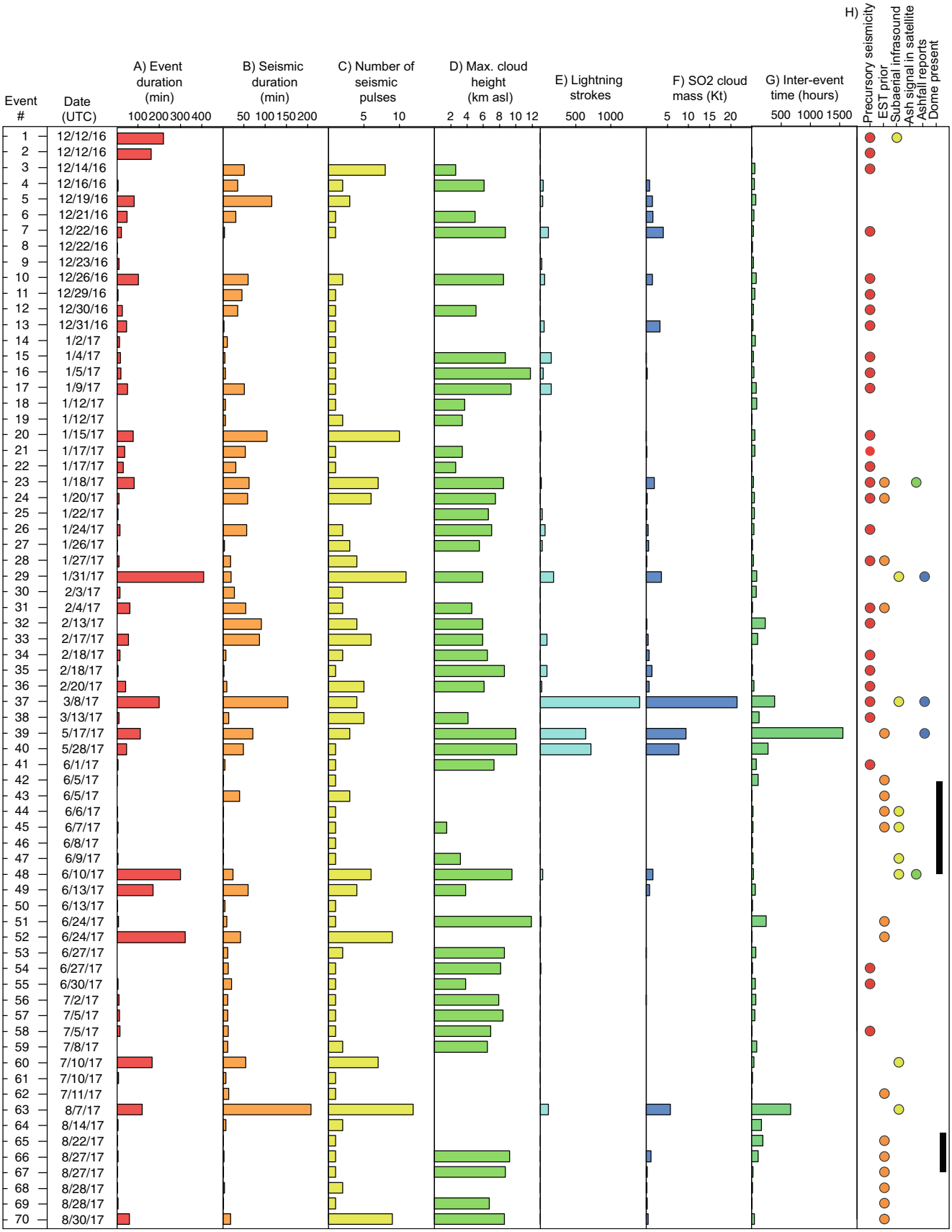
Event #
Date (UTC)
A) Event duration (min)
100 200 300 400
B) Seismic duration (min)
50 100 150 200
C) Number of seismic pulses
5 10
D) Max. cloud height (km asl)
2 4 6 8 10 12
E) Lightning strokes
500 1000
F) SO2 cloud mass (Kt)
5 10 15 20
G) Inter-event time (hours)
500 1000 1500
H)
Precursory seismicity
EST prior
Subaerial infrasound
Ash signal in satellite
Ashfall reports
Dome present
1 12/12/16
2 12/12/16
3 12/14/16
4 12/16/16
5 12/19/16
6 12/21/16
7 12/22/16
8 12/22/16
9 12/23/16
10 12/26/16
11 12/29/16
12 12/30/16
13 12/31/16
14 1/2/17
15 1/4/17
16 1/5/17
17 1/9/17
18 1/12/17
19 1/12/17
20 1/15/17
21 1/17/17
22 1/17/17
23 1/18/17
24 1/20/17
25 1/22/17
26 1/24/17
27 1/26/17
28 1/27/17
29 1/31/17
30 2/3/17
31 2/4/17
32 2/13/17
33 2/17/17
34 2/18/17
35 2/18/17
36 2/20/17
37 3/8/17
38 3/13/17
39 5/17/17
40 5/28/17
41 6/1/17
42 6/5/17
43 6/5/17
44 6/6/17
45 6/7/17
46 6/8/17
47 6/9/17
48 6/10/17
49 6/13/17
50 6/13/17
51 6/24/17
52 6/24/17
53 6/27/17
54 6/27/17
55 6/30/17
56 7/2/17
57 7/5/17
58 7/5/17
59 7/8/17
60 7/10/17
61 7/10/17
62 7/11/17
63 8/7/17
64 8/14/17
65 8/22/17
66 8/27/17
67 8/27/17
68 8/28/17
69 8/28/17
70 8/30/17

◀ **Fig. 8** Overview of eruption parameters for 70 explosive events that occurred during the 2016–2017 eruption of Bogoslof volcano. Because of the wide range of values for some parameters, smaller values may not always show up graphically here; all data are also given in Table 1. **a** Event duration as determined by infrasound data, in minutes, shown by solid red bars. **b** Seismic duration, in minutes, shown by solid orange bars. **c** Number of seismic pulses. **d** Maximum cloud height in kilometers above sea level, when known, as determined by satellite data. **e** Number of lightning strokes as detected by the Vaisala Network, shown in cyan bars. **f** SO_2 cloud mass, in kilotons, as determined by satellite in blue bars. **g** Inter-event time, in hours. **h** Presence of precursory seismicity, elevated surface temperatures (EST), subaerial infrasound, ash signal in satellite, and ashfall reports indicated by solid circles; presence of subaerial dome showed by black bars. Data and data sources for a–f are given in Table 1. Precursory seismicity from Tepp and Haney (2019), subaerial infrasound from Fee et al. (2019), and ash signal from Schneider et al. (2019). EST dates are shown in Electronic Supplement

circular craters. The one to the northwest had upwelling within it, suggesting it was above the vent for the event 26 explosion (Waythomas et al. 2019a, their Fig. 8).

Event 29 (January 31: sustained eruption from a subaerial vent)

About 84 h after event 28, the longest sustained explosion of the eruptive sequence produced significant ash and resulted dramatic changes to Bogoslof Island. **Event 29** comprised more than 10 short-duration explosions that were detected in seismic, infrasound, and lightning data, took place over several hours on January 31, and produced several discrete volcanic clouds.

The event started with no detected precursors, and activity escalated from 08:40 to 09:30, as indicated by increased seismic tremor and high amplitude infrasound signals. At 09:00, a continuous volcanic plume extended for a distance of more than 200 km towards the east-southeast over Unalaska Island at an altitude of 5.9 km asl. Event 29 produced 190 lightning strokes (Table 1; Van Eaton et al. 2019) and the most significant SO_2 emission since December 22, 2016 (3.6 kt; Lopez et al. 2019).

Tephra accumulation at the vent produced a demonstrably dry volcanic edifice for the first time during event 29. Data derived from US National Imagery Systems shortly after the event showed light steaming from an apparently dry eruption crater about 400 m in diameter and as much as 100 m deep below the west crater rim. Whereas most previous explosive events in the sequence, with the possible exception of event 23 on January 18, issued from a vent in shallow seawater, freshly erupted tephra formed an almost 200-m-wide barrier separating the vent from the sea. A Worldview-3 image from about 15 h later the same day (Fig. 6d) shows that the crater had already begun to fill with seawater. As with several of the events, large ballistic blocks were visible along the island's north southwest shoreline (Waythomas et al. 2019a, their Fig. 9).

Event 29 resulted in ashfall on Unalaska Island including trace (< 0.8 mm) amounts in the community of Dutch Harbor/Unalaska. A sample of ash collected in Dutch Harbor comprises free crystals of plagioclase, clinopyroxene, amphibole, and rare biotite, as well as particles that display a range of groundmass textures from microlitic to glassy, and that vary from dense to vesicular (Loewen et al. 2019). The material is consistent with being a mixture of juvenile basalt scoria and non-juvenile lithics.

Events 30–36 (February 3–20: low-level explosive activity)

Following event 29, a series of smaller explosive events occurred from February 3 to 20 (events 30–36; Table 1). During this period, the inter-event times became more variable, with some pauses of up to 9 days between events. Explosions during this time lasted minutes to a few tens of minutes, produced clouds that rose from 4.6 to 8.6 km asl (Schneider et al. 2019), 0–92 strokes of lightning (Van Eaton et al. 2019), and modest SO_2 (0–1.4 kt; Lopez et al. 2019).

A series of satellite images from January 31 through February 12 shows little change in the island's morphology after event 29 (Fig. 6d–e; Waythomas et al. 2019a). Elevated surface temperatures detected in two MODIS images from February 6 likely reflected hot new deposits from event 31 on February 4. A high-resolution Worldview-2 satellite image from February 23 also shows little change except for the presence of ballistics particles ejected during events 32–36 (February 13–20) and distributed across the island (Waythomas et al. 2019a). A clear view from March 3 similarly shows only minor changes (Fig. 6f).

The final event in this time interval, **event 36** on February 20, was an excellent example of a Bogoslof explosion with a precursory seismic sequence (see Fig. 4 of Coombs et al. 2018). A classic sequence of coalescing earthquakes served as a prelude to the series of energetic eruptive signals that made up the event. Earthquakes were first detected at 20:42 on February 19. The sequence then maintained a relatively low rate until about 00:55 (February 20) when the rate suddenly increased to about 30 earthquakes per hour. The rate then progressively increased over the next hour almost merging to tremor by 2:00. Earthquakes ceased at 2:07 and after a 1-min break transitioned to tremor. The eruptive signals consisted of about 9 blasts that were captured on multiple infrasound arrays resulting in a 40-min long explosion. The resulting plume reached 6.1 km asl and was elongated, stretching to the east-southeast over Unalaska Island. Pilots and observers on Unalaska Island at the time clearly observed the white, ice-rich cloud (Fig. 4e).

Event 37 (March 8: long duration and ashy)

After a 16-day pause, **event 37** on March 8 lasted 200 min. It had the largest infrasound energy (Lyons et al. 2019a), seismic tremor magnitude (Tepp et al. 2019), most lightning (1437 strokes; Van Eaton et al. 2019), largest SO_2 emission (21.5 kt; Lopez et al. 2019), and most significant ash cloud (Schneider et al. 2019) of any event in the eruptive sequence (though not the highest reduced displacement; Haney et al. 2019a). VIIRS satellite images showed the resulting cloud reached between 10.6 and 13.4 km asl and drifted east over Unalaska Island. Minor ashfall of a few millimeters was reported by a mariner near Cape Kovrizkha (northwest Unalaska Island; Fig. 1) who collected ash from his vessel. Like the ash sample from January 31, this ash contains particles of juvenile basaltic scoria and free crystals with minor amounts of what appear to be volcanic lithics (Loewen et al. 2019). A barely perceptible ashfall deposit was reported at Unalaska/Dutch Harbor.

Event 37 also changed the shape of the island and temporarily dried out the vent area, as seen in a Landsat-8 image from March 8 (not shown). In infrasound data, event 37 shows a mix of low and high FI, consistent with an eruption from both submarine and subaerial vent(s) during this event (Fee et al. 2019).

A March 11 WorldView-3 image (Fig. 6g) shows the west coast of the island grew significantly since March 3 (Fig 6f), with about 250 m of new land west of the 1926–1927 dome. A new ~ 150-m wide vent was also observed on the north coast of the island, and ballistics ejecta clustered on the eastern side of the island (Waythomas et al. 2019a, their Fig. 11).

Event 38 and preceding swarms (March 10–13)

On March 10 and 11, two multi-hour seismic swarms each produced hundreds of earthquakes as detected on station MAPS (Tepp et al. 2019), but neither led directly to an explosion. A few hours later, a precursory swarm (Tepp et al. 2019) began on March 11 and culminated on March 13 in **event 38**. This event produced a small cloud that reached as high as 4.1 km asl and drifted south-southwest.

Explosive hiatus (March 13–May 16)

Following event 38 on March 13, there was a 9-week pause in explosive activity at Bogoslof. The only detected unrest observed during the hiatus was a swarm of volcano-tectonic earthquakes on April 15. The swarm lasted for several hours, comprised 118 detected earthquakes (catalog of Wech et al. 2018) with magnitudes between ~ 0.8 and 2.2, and is interpreted to reflect magmatic intrusion in the mid to upper crust because of the earthquakes' weak *T*-phases (Wech et al. 2018).

Satellite images from this period show the rapid surface reworking and erosion of new volcanic deposits on Bogoslof Island and coastline erosion by wave action (Waythomas et al. 2019a). Photos (Fig. 5a) and a Worldview-3 image from May 11 (Fig. 6h) show that the vent lagoon remained hot throughout the hiatus, evidenced by steam rising from the crater lagoon.

Phase 2: renewed explosive activity and dome building (May 17–August 30)

From May 16 through August 30, AVO detected 32 explosive events at the volcano. In contrast to the events of December 2016–March 2017, few of the explosions in the later phase were preceded by detectable seismic precursors, inhibiting AVO's ability to forecast eruptive activity (Coombs et al. 2018), though retrospective analysis of hydrophone data showed that weaker precursors were still often present (Tepp et al. 2019). Fewer events produced detectable lightning after event 40 on May 28 (Van Eaton et al. 2019). This second phase also included effusion of two short-lived subaerial lava domes.

Events 39 and 40 (May 17 and 28: energetic events after a pause)

After a nine-week hiatus, Bogoslof erupted without detectable geophysical precursors on May 17 (event 39). This explosion lasted 200 min and produced an ash cloud that reached as high as 10 km asl and drifted south along the edge of a mass of weather clouds, as seen in GOES satellite imagery (Schneider et al. 2019) and reported by pilots. Trace ashfall (< 0.8 mm) was reported in Nikolski, Alaska, 123 km southwest of Bogoslof (Fig. 1). As with ash samples from the previous two events, this one contains about 40 % free crystals, though the remainder of this sample is richer in juvenile scoria (as opposed to lithic fragments) than previous ones (Loewen et al. 2019).

Following **event 39**, an oblique photo showed that the crater lake was breached with a 550-m wide gap along the north shore and that the northeast shore was extended by another 300 m from new tephra deposits (Fig. 5b). Eleven days after event 39, explosive **event 40** occurred on May 28, also with no detected precursors. This eruption produced an ash cloud that rose to 10.1 km asl as shown in MODIS satellite images (Schneider et al. 2019). The cloud drifted to the northeast and was reported by numerous pilots, including a report of "sulfur smell in cockpit" from a plane about 800 km from Bogoslof. A Worldview-3 satellite image collected about 18 min after the start of the event shows the initial development of the eruption cloud (Fig. 4f; Waythomas et al. 2019a).

These two explosive events, which occurred just after the hiatus, are among the most energetic of the eruptive sequence. They both produced appreciable SO_2 clouds as detected in

satellite data (9.4 and 7.7 kt; Lopez et al. 2019) and generated among the highest number of lightning strokes (647 and 719; Van Eaton et al. 2019; Fig. 8). The remnant SO_2 cloud from event 40 on May 28 was still detectable over Hudson Bay, over 4000 km east of Bogoslof, on June 2. Of the 25 events analyzed by Haney et al. (2019a), the co-eruptive tremor of these two events had the highest reduced displacement of any in the sequence—both yield values of about 50 cm^2, which is comparable to values calculated for eruption tremor from the largest eruptions in Alaska over the past 20 years (e.g., Redoubt in 2009; McNutt et al. 2013).

Cosmo SkyMed radar imagery from May 31 shows a large portion of the north side of the island was removed during May 28 explosive activity, leaving a crescent-shaped bay, open to the north. This configuration of the island remained essentially intact through June 12 (Fig. 6i).

As seen previously from a March 8 Landsat image, sometime following May 28, intense steaming recommenced from an area just southwest of the vent lagoon. This region, about 300 m in diameter, remained hot and emitting steam throughout the eruption and afterwards (Fig. 6i–l), and may have been the site of shallow magma intrusion or a filled-in vent area.

June lava dome and small events 41–47 (June 1–9)

Early June brought a series of small explosions and growth of a lava dome that breached sea level on June 5, and was then destroyed on June 10.

Several hours after a swarm of very small earthquakes on May 31, **event 41** was a 5-min long explosion that produced a small, water-rich cloud that reached as high as 7.3 km asl. Following this, cloudy weather prevented clear views of the volcano through June 4. A Sentinel 1-B SAR image from June 4 shows no dome in the crater lagoon (Fig. 7a). Midday on June 5, data derived from US National Imagery Systems indicate that a small protrusion of lava had breached water level immediately between the 1926–1927 and 1992 lava domes in northern portion of vent lagoon. By June 6, low-resolution satellite images show distinctly elevated surface temperatures at Bogoslof, suggesting that hot lava was at the surface (Fig. 8). Sentinel-1 SAR images show the growth of the dome from June 7 through June 9 (Fig. 7b,c). On June 7, data derived from US National Imagery Systems showed that the new dome was about 110 m in diameter. The dome was also seen in a COSMO SkyMed radar image from June 8 (Waythomas et al. 2019a; their Figure 15).

During the interval of lava effusion, several small explosive events (**42–47**) occurred that did not disrupt the growing dome as shown by Sentinel-1 SAR data from June 9, which confirmed that dome was still there after event 47 (Fig. 7c). Several of the events (44, 45, and 47) have infrasound frequencies consistent with a subaerial vent (Fee et al. 2019).

Event 48 (June 10: dome destroying event)

The June 5 lava dome was short-lived, as it was completely destroyed during a long, pulsatory explosive event on June 10 (**event 48**). This event started with discrete explosions detected on the Okmok infrasound array as early as 8:27 but intensifying from 11:18 to 11:38. Starting at about 12:16, activity transitioned into nearly continuous seismic and infrasound tremor signals for about 40 min. Shorter bursts of tremor continued until 14:51, for an envelope of activity that lasted several hours. VIIRS satellite images of the resulting cloud showed it reached as high as 9.5 km asl and drifted to the northwest. Satellite data also indicated that at least part of the volcanic cloud was more ash-rich than many of those seen previously in the Bogoslof eruptive sequence to date, suggesting that the eruption may have fragmented and incorporated the lava dome that was emplaced earlier that week (Schneider et al. 2019). This event generated 31 detected lightning strokes (Van Eaton et al. 2019).

A Worldview-3 image from June 10, acquired after event 48, shows that the June 5 dome was no longer present (Waythomas et al. 2019a). Another, clearer Worldview-3 image from June 12 (Fig. 6i) showed ballistic blocks distributed uniformly around the island with the highest concentrations in the southeast and southwest sectors—likely remnants of the June 5 dome (Waythomas et al. 2019a). The FI of infrasound from this event gradually decreases in the last hour of the event, suggesting a change from subaerial to submarine venting after the destruction of the lava dome (Fee et al. 2019; their Fig. 8).

Events 49–62 (June 13 to July 11: small explosions)

On June 13, **event 49** comprised a series of four explosions that started at 01:44 and ended at about 04:34. Each pulse lasted between 10 and 30 min and generated volcanic clouds that rose to a maximum height of 3.8 km asl and dissipated within about 30 min. Residents of Unalaska/Dutch Harbor reported smelling sulfur, and winds were consistent with a source at Bogoslof. An additional 2-min long explosion was detected in seismic and infrasound data later on 13 June (**event 50**), with no detected ash cloud.

There was an 11-day pause in detected explosive activity from June 13–24. During an overflight on June 22, sediment-laden water was visible in the open vent lagoon area, and the area of persistent steaming was visible just east of the December uplift area (Fig. 5c).

Twelve explosive events occurred from June 24 to July 11 (**events 51–62**). These were generally short-duration, detected in seismic and infrasound data, and produced little or no lightning (Table 1). Several of these events were closely spaced groups of smaller events. A photo taken on July 3 shows the area of

persistent steaming visible from behind the December uplifted block, but no activity at other areas of the island (Fig. 5d).

Event 63 (August 7: long duration and ashy)

Following an almost month-long pause, explosive activity resumed on August 7, with a 2-h long sequence (**event 63**; Table 1). Detected in seismic, infrasound, satellite, and lightning data, event 63 was longer lived than many of the events in the eruptive sequence and satellite images showed that ash from the eruption formed a continuous cloud that was carried by strong winds south over Umnak Island and then out over the Pacific Ocean reaching an altitude of 10–12 km asl (Schneider et al. 2019). Event 63 produced one of the largest SO_2 masses of the eruption, 5.8 kt, as determined by IASI satellite (Lopez et al. 2019). It also yielded the highest number of lightning strokes during the second half of the eruption (117; Van Eaton et al. 2019).

As shown in a Worldview-2 image from August 8 (Fig. 6j), event 63 produced significant proximal tephra that expanded Bogoslof Island's northern coastline and closed off the north-facing lagoon to create a crater lake in the vent region, perhaps even leading to a subaerial vent for some portion of this explosive event. This image also shows a large number of new ballistic blocks, primarily in the east-southeast sector of the island (Waythomas et al. 2019a, their Fig. 18). In infrasound data, event 63 shows a progression from low to high FI, consistent with a shift from submarine to subaerial venting (Fee et al. 2019).

August lava dome, events 64–70 (August 14–30)

The final 2 weeks of the eruption were marked by mostly short-duration explosions and concurrent growth of a lava dome. **Events 64 through 70** were mostly short-lived (6 min or less, except event 70 which lasted 59 min; Table 1), produced little or no lightning (Van Eaton et al. 2019), and modest SO_2 (up to 1.2 kt; Lopez et al. 2019). Volcanic clouds from the explosions rose to high altitudes (up to 8.7 km asl; Schneider et al. 2019) despite their short durations.

A high-resolution Worldview-3 image on August 13 shows a vent region filled with seawater and no lava dome was apparent (Fig. 6k). On August 15, repeating low-frequency seismic events from Bogoslof were detected on Okmok and Makushin networks for about 8 h (Tepp et al. 2019). A photo from an overflight of the volcano on August 15 shows the area of persistent steaming visible since late May, but nothing at the site of the dome that would appear days later in the vent lagoon (Fig. 5e). If the August 15 seismicity was related to magma ascent, it had not yet risen shallowly enough to impact the vent lagoon area.

A new lava dome was observed in data derived from US National Imagery Systems in the enclosed, water-filled crater on August 18 and grew to about 160 m in diameter and 20 m tall by August 22. A Sentinel SAR view shows the dome on August 20 (Fig. 7d). An oblique aerial photo taken on August 26 shows a vigorous steam plume that likely was generated as hot dome rock interacted with seawater in the vent lagoon area (Fig. 5f).

SAR images from Sentinel-1 (Fig. 7e) and Cosmos SkyMed (Fig. 7f) on August 27, after event 66, suggest that most of this dome had been removed, with only some northern dome edge remnants remaining. The low-frequency infrasound associated with events 66–69 suggest that the vent was below water (Fee et al. 2019).

Eruption end and continuing quiescence

Following the last explosive activity on August 30, there were a few earthquakes detected in seismic and hydrophone data (G. Tepp, written comm. 2019), but seismic activity quieted soon after. In August 2018, AVO added a telemetered seismometer on Bogoslof Island, which has recorded little activity of note.

Weakly elevated surface temperatures were consistently observed at Bogoslof in low-resolution satellite images through November 2017. High-resolution satellite images from the fall of 2017 show steaming and discoloration on the island (e.g., Fig. 6l). As of 2019, continued erosion has changed the shape of the island (Waythomas et al. 2019b), similar to what occurred following previous eruptions.

Overview and synthesis

Magma generation and ascent

We know little about the upper crustal magmatic storage system at Bogoslof due to the lack of local geophysics and detailed petrologic studies. Erupted compositions of (trachy)basalt through trachyte are typical for a back-arc source (Churikova et al. 2001). Trace element ratios in Bogoslof basalts suggest that their mantle source likely had more residual garnet (and are thus deeper) and resulted from lower degrees of partial melting than nearby arc-front volcanoes (Loewen et al. 2019). The dominant juvenile component in 2016–2017 was an amphibole-bearing basalt with a mineral assemblage suggestive of shallow crustal storage at less than 100 MPa; matrix glass heterogeneity also requires multiple inputs from depth or rejuvenation of shallowly stored basalts (Loewen et al. 2019).

Seismicity provides a clue about when the juvenile basalt may have mobilized beneath the volcano. Starting in September 2016, Bogoslof was fed by several hours-to-day-long episodic intrusions in the middle to upper crust marked

by non-eruptive relatively deep earthquake swarms (Wech et al. 2018).

In addition to the dominant basalt, other compositions that erupted in 2016–2017 may be residual from previous eruptions.The similarity of 2016–2017 trachyte pumice composition to the 1796 Castle Rock period suggests this may be a rejuvenated magma from that previous episode; large complex zoned sanidine phenocrysts, eutectic plagioclase-sanidine-quartz equilibrium, and accessory titanite growth are consistent with protracted shallow storage (Loewen et al. 2019). Some variation in 2016–2017 basalts could be due to rejuvenation and incorporation of 1992 or other recently erupted basalts (Loewen et al. 2019). The northwest-southeast alignment of multiple vents that were active in 2016–2017 suggests shallow dike emplacement, which may have facilitated interaction with these shallowly stored bodies.

Precursory seismicity provides some clues about the final stages of magma ascent prior to explosive eruptions. During the first half of the eruption starting in December 2016, sequences of strong repeating earthquakes at the base of the volcano heralded explosions, as magma ascended a few kilometers on time scales of minutes to hours (Wech et al. 2018). Following June 1, few of the events had detectable precursors (Wech et al. 2018; Tepp and Haney 2019) though weaker precursory seismicity was detected on a proximal hydrophone installed in May 2017 (Tepp et al. 2019). Wech et al. (2018) suggest early swarms and eruptions created an open pathway allowing subsequent intrusions to reach the surface aseismically (as measured distally), which explains the termination of precursory earthquakes. This is also consistent with decreasing proportions of non-juvenile lithics with time for the three sampled ash deposits (though, last ash sample is from May 17; Loewen et al. 2019).

Near-vent processes and the role of seawater

Perhaps the most notable feature of this 9-month long eruption was the vent location in shallow seawater and the effects on eruptive style. As is common for explosive eruptions that occur in oceanic, lacustrine, or glacial settings (Mastin and Witter 2000), Bogoslof produced volcanic clouds that show evidence for entrainment of large amounts of water from the vent region (Schneider et al. 2019). Most volcanic clouds generated during the Bogoslof eruption were described as water-rich based on spectral properties and white color; however, it is not known whether these water-rich clouds were in fact ash-poor or if condensed water and/or ice growth encased or otherwise obscured the presence of volcanic ash. Further evidence for the role of seawater are low SO_2 masses for many of the events; because SO_2 is soluble in water, it may have been scrubbed from the gas phase during wholly submarine explosions (Lopez et al. 2019).

Despite the notable character of many of the volcanic clouds, and clear evidence for seawater interaction, questions remain about the overriding mechanism driving the explosive activity at Bogoslof. Were explosions dominantly magmatic, phreatic, or phreatomagmatic? Was fragmentation driven by magmatic degassing the primary driver of explosive activity? Did magma typically encounter seawater at a relatively restricted interface as a submarine plug or dome, or as magma moved toward the surface, did it encounter water-saturated, unconsolidated material in a funnel-shaped vent containing a water-saturated mixture of volcaniclastic debris as described by Kokelaar (1983) and proposed by Waythomas et al. (2019b)? Because the latter type of mechanism generates continuous expansion as opposed to explosions, it does not seem consistent with the observations we have at Bogoslof, which show a series of sudden and discrete explosive events. Important to remember is that we missed much lower level activity due to the veil of distance, poor weather, and darkness. Classic Surtseyan activity, with accompanying "cock's tail" tephra jets (Houghton et al. 2015), may have occurred at Bogoslof unseen and undetected.

The majority of activity that we could observe and detect consisted of repetitive, short explosions, with subordinate dome effusion; and a small number of longer, more sustained and ash-rich explosive events. The cyclic events that dominated the eruptive sequence are consistent with vulcanian activity, which is attributed to cyclic build-up and release of pressure below a plug of degassed magma in the shallow conduit or as a dome (Druitt et al. 2002). While sampling throughout the 2016–2017 Bogoslof eruption was not possible, those samples that have been collected are texturally consistent with fragmentation driven by magmatic volatiles, with seawater interaction playing a subordinate role (Loewen et al. 2019). Pervasive breakdown rims on amphibole phenocrysts and variable but generally high microlite contents (Loewen et al. 2019) are consistent with slow ascent to, and/or stalling out at, shallow levels within the conduit (Rutherford and Hill 1993; Clarke et al. 2007). Ballistic dispersal patterns that are not symmetrical around the vent, while not necessarily unusual, suggest non-vertical directionality to the explosions (Waythomas and Mastin 2019), which may be related to disruption of portions of a solidified dome or plug at the top of the conduit.

Similarly, analysis of infrasound data suggested that while seawater plays a role, explosions appear to have been driven by magmatic volatiles. Lyons et al. (2019a) conclude that for some of the explosions, seawater acts to produce a gas-tight seal near the vent, as degassing juvenile magma ascends in the upper conduit. As this magma dome or plug is disrupted—likely by overpressurization from below, perhaps combined with infiltration of seawater from above—the release of large, bubble-forming volumes of gas are released. Lyons et al. (2019a) describe the resultant eruptive style as hydrovulcanian.

Several parameters that changed during the course of the eruption appear related to the development of the growing island and a transition from a mostly submarine to a partially subaerial eruption. Before January 18, no thermal signatures were seen in satellite data (Fig. 8), and other than event 1, no subaerial-type infrasound (i.e., FI > − 1) was seen until event 29 on January 31 (Fee et al. 2019). Note that Okmok infrasound data were not available on January 18 for event 23, and thus FI was not calculated for this event (D. Fee, written comm. 2019), which showed other signs of subaerial venting. Taken together, along with satellite images of the growing island (Fig. 6), these lines of evidence document the development of a growing shallow-to-subaerial edifice that perhaps minimized the extent of interaction between seawater and ascending magma.

This development may be reflected in a transition in the pace of explosive activity. During the first few weeks of the eruption through February 4, there was a high rate of explosive activity, with one event on average every 1.7 days (Fig. 8). This suggests gas-rich magma was ascending and pressurizing behind plugs rapidly cooled by seawater (Searcy and Power 2019). As the eruption progressed, inter-event time generally became more variable and increased (Fig. 8).

The four events that were preceded by inter-event times of more than 10 days (events 37, 39, 40, and 63) have the highest SO_2 masses (Lopez et al. 2019), elevated lightning (Van Eaton et al. 2019), and some of the longest seismic durations (Searcy and Power 2019). As pointed out by Searcy and Power (2019), this is consistent with observations of longer inter-event intervals corresponding to more energetic eruptions at other volcanoes (e.g., Montserrat; Druitt et al. 2002), perhaps owing to greater pressurization beneath a sealed plug or dome.

Hazards, impacts, and mitigation measures

Bogoslof is remote, unpopulated, and within the Alaska Maritime National Wildlife Refuge, therefore proximal hazards such as pyroclastic flows and surges, ballistics, mud rain, and submarine explosions (Waythomas and Cameron 2018) typically only affect marine life. Sea lions and other marine animals may be harmed (Merriam 1901) during eruptions of Bogoslof, but rapidly return to the island during quiescence (Sobel 2017). Distal hazards at Bogoslof during the 2016–2017 eruption were primarily caused by volcanic ash clouds and ashfall. Ash clouds and ashfall from Bogoslof explosions posed a threat to local and North Pacific aviation, nearby communities including Unalaska/Dutch Harbor and Akutan and the fishing industry they support, and marine vessels.

Airborne ash and aviation

During the 1992 and 2016–2017 eruptions of Bogoslof, volcanic clouds were observed drifting downwind for 100s of kilometers from the island. These volcanic clouds pose significant hazards to aircraft that may fly through them (Guffanti et al. 2010). More than 60,000 passengers transit the airspace above Alaska volcanoes in a given day (Ewert et al. 2018).

The best mitigation measure for aviation hazards is timely notification of eruptive activity. Bogoslof highlighted the challenges in volcano monitoring in Alaska and other areas where ground-based monitoring is absent, and the volcano is remote. Coombs et al. (2018) describe the operational tools and protocols developed and used during the eruption, including automated alarms for seismic, infrasound, lightning, and remote-sensing data, as well as pilot reports, and rapid tools for intra-observatory communication (AVOChat; since expanded to use at HVO during the 2018 Kilauea eruption; Neal et al. 2018). During the eruption, AVO raised the aviation color code (Guffanti and Miller 2013) to RED 30 times, was at ORANGE for most of the sequence (Fig. 2), and issued 228 event-driven (as opposed to scheduled) notices of volcanic activity to the public and other agencies. Of the 70 explosive events for which notifications were issued, aviation authorities were notified by phone an average of 22 min after the event, and written notices were issued an average of 37 min after onset (Coombs et al. 2018). For events that produced clouds higher than 7.5 km asl, these averages drop to 15 and 30 min, respectively. This improvement in timeliness is because larger events are typically seen in more data streams, decreasing uncertainty about the existence and character of the eruption.

During the 2016–2017 eruption of Bogoslof, especially the first 2 months, the FAA diverted air traffic around Bogoslof volcanic clouds, and regional flights to and from Dutch Harbor were typically canceled during explosive periods. The FAA created a temporary flight restriction (TFR) of 10 nautical miles and 12.2 km asl around the volcano from January 10 to October 9, with a short break in early May (when it appeared that the eruption may have ended). Event-driven Volcanic Ash Advisories were issued by the Anchorage Volcanic Ash Advisory Center (VAAC) numerous times (Fig. 9). AVO worked closely with the VAAC before and during ash-producing events to coordinate on timing and distribution of explosive events, and interpretation of satellite and lightning data.

We do not know the total number of impacted flights, but on January 18 alone at least 50 aircraft were rerouted to avoid volcanic clouds from Bogoslof (National Weather Service [NWS] Center Weather Service Unit written comm. 2017). Multiple flights were impacted during and after the March 8 event (NWS-CWSU, written comm. 2017). Bogoslof volcanic clouds continued to affect aviation well into summer 2017, as Bogoslof was blamed for flight delays and cancelations that reduced Asia-to-US air freight capacity (Cheshire 2017).

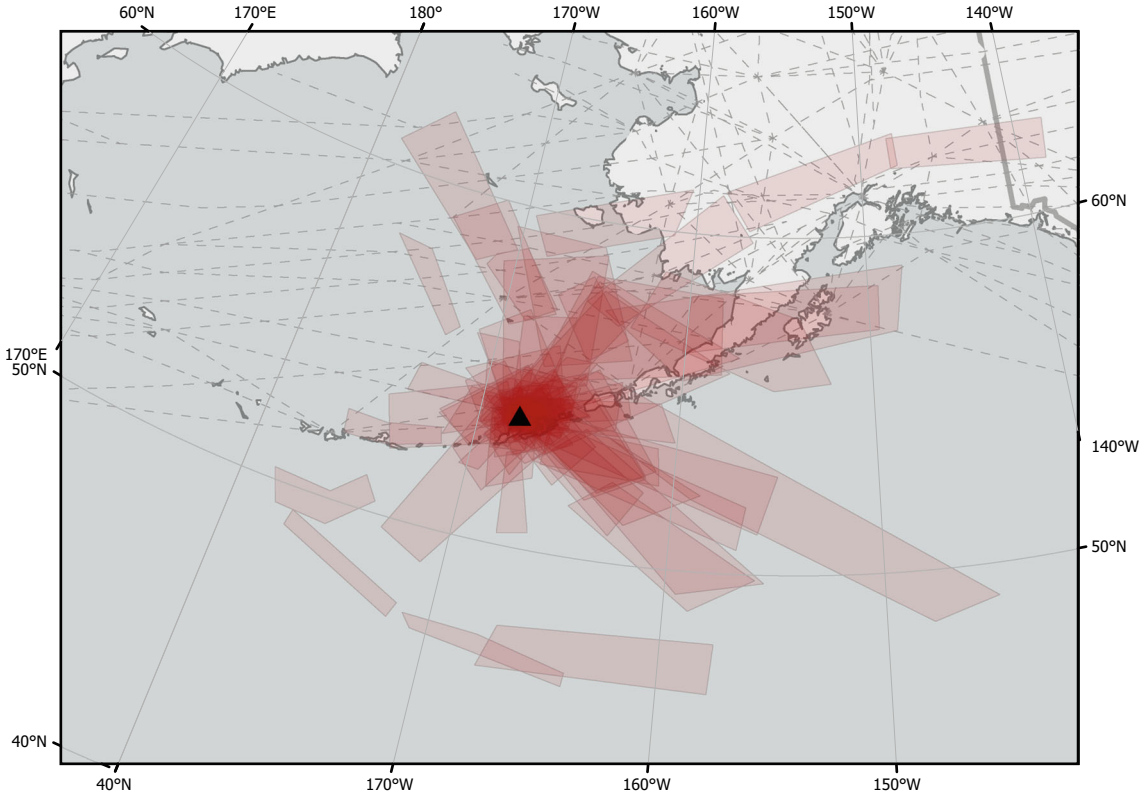

Fig. 9 Map of the North Pacific showing discrete areas of airborne volcanic ash (in red) reported by the Anchorage Volcanic Ash Advisory Center (VAAC based on satellite imagery, pilot reports, eye-witness accounts, and other data, for the time period December 2016 through August 2017. Over the course of the 2016–2017 eruption of Bogoslof volcano the Anchorage VAAC released more than 100 Volcano Ash Advisories, most of which included 24 h forecasts about likely plume trajectories and dispersion rates. Dashed lines show fixed high-level air routes in the region

Ashfall

Historical eruptions of Bogoslof have produced trace (< 0.8 mm) to minor (0.8–6.4 mm) amounts of ashfall on nearby communities and mariners, including the 1796, 1882, 1907, and 2016–2017 eruptions (Waythomas and Cameron 2018). These amounts of ashfall may cause infrastructure problems, require clean up, impair drinking water systems, harm machinery, or cause eye and respiratory irritation (Wilson et al. 2012; Horwell and Baxter 2006; https://volcanoes.usgs.gov/volcanic_ash/). During the recent eruption, trace amounts of volcanic ash fell on communities during three explosive events. Trace ashfall at Dutch Harbor/Unalaska on January 31, easily apparent on snow and vehicle surfaces (Fig. 10a), rendered the runways, taxiways, and airport ramps unusable until the ash was cleaned from those surfaces using a hose. On March 8, a mariner near Cape Kovrizkha (northwest Unalaska Island) reported minor ash on his vessel (Fig. 10b). Residents of Dutch Harbor and Unalaska also reported trace ashfall on March 8, describing it as a very small amount (grains versus a continuous deposit), best viewed on car surfaces. On May 17, residents of Nikolski, about 123 km (76 mi) southwest of Bogoslof, reported trace ashfall (Fig. 10c). AVO received numerous reports of trace ashfall from the events via phone, email, and its online ash reporting system, Is Ash Falling? (https://avo.alaska.edu/ashfall/ashreport.php).

The U.S. Geological Survey (USGS) provides forecasts of expected ash dispersion (ash clouds) and deposition (ashfall) from volcanic eruptions using the numerical atmospheric transport model Ash3D (Schwaiger et al. 2012). The 2016–2017 Bogoslof eruption was the first in the USA for which Ash3D was used routinely in response mode. Event-specific simulations were initially run with a known start time and estimated plume height and duration, but then run iteratively as new information was available. AVO communicated Ash3D ash fallout results directly with the NWS Forecast Office who has the responsibility to issue ashfall warning to communities and mariners.

The three events when ashfall affected communities were well simulated using Ash3D (Fig. 11), facilitating hazard notification to the public. Since the vast majority of ashfalls were onto marine waters and the Bering Sea is home to the largest fishing industry in North America as well as transportation routes, numerous NWS Marine Weather Statements were issued based on Ash3D model output, warning mariners of ash fallout.

Fig. 10 Photographs of distal ashfall from the 2016–2017 eruption of Bogoslof volcano. **a** Ashfall deposit on car hood, which was produced during explosive event 29 on January 31 in Unalaska, Alaska. Photo courtesy of Tom Cohenour. **b** Sample of volcanic ash from event 36 on March 8, 2017, collected by Trevor Shaishnikoff of Unalaska. The ash was collected from the roof of the wheelhouse of his boat near Cape Kovrizhka when the ashfall occurred at about 05:30 AKST. **c** Trace ashfall on all-terrain vehicle in the community of Nikolski from explosive event 39 on May 17. Photo courtesy of Lilly Stamm

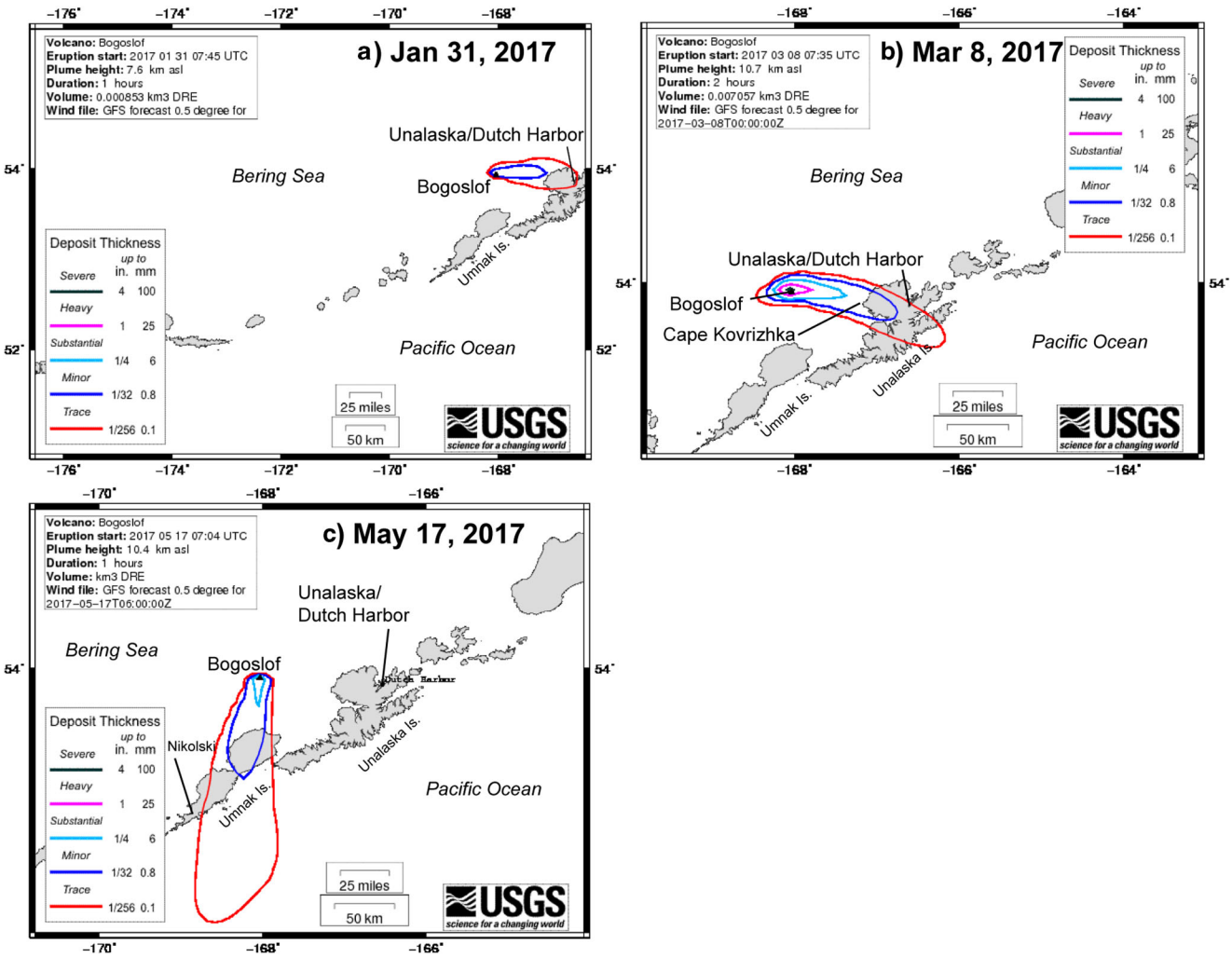

Fig. 11 Ash3D model results shown on AVO public webpage for the three ashfall events that impacted communities during the Bogoslof 2016–2017 eruption, **a** January 31, 2017—Dutch Harbor/Unalaska; **b** March 8, 2017—Unalaska Island and Cape Kovrizhka; **c** May 17, 2017—Nikolski

Marine hazards

Bogoslof is 100 km from Dutch Harbor/Unalaska, the top commercial fishing port in the USA (National Marine Fisheries Service 2017) and 150 km from Akutan, home to a large fish processing facility. Thus, there was significant concern that ashfalls on these communities, and the surrounding fishing grounds of the Bering Sea and nearby Pacific Ocean, could have great impact on the fishing industry. The US Coast Guard issued a Local Notice to Mariners (LNTM) warning of proximal hazards, extending through most of the eruptive period—late January through June—recommending a safe distance of more than 10 km from Bogoslof Island. Numerous ashfall warnings were issued by the NWS Forecast Office to mariners navigating the vast fishing grounds and shipping lanes (Marine Weather Statements) and to communities (Special Weather Statement) where ashfall was expected based on weather patterns, Ash3D simulations, and coordination with AVO. To our knowledge, ashfall did not cause notable problems for mariners, likely due to issued warnings, and AVO received only a single report of ashfall on a vessel.

Community engagement

During the eruption AVO staff visited Dutch Harbor/Unalaska, the largest population center in the Aleutian Islands, to deploy instruments, perform network maintenance, map and collect ash deposits, and set up a particulate monitor to assess air quality associated with potential ashfall. AVO interacted with the community through public talks, radio interviews, and numerous ash-collection workshops at local schools. AVO visited the local clinic, the water treatment and wastewater facility, the Public Works office (roads and facilities), a seafood processing plant, and several fishermen with the goal of sharing resources, answering questions, and improving communication, education, and training. Following several of the larger explosive events, AVO provided expert guidance on activity and hazards during community calls organized by the State of Alaska Department of Homeland Security and Emergency Management.

Warnings about volcanic explosions at Bogoslof successfully aided emergency managers, aviation personnel, and communities to protect aircraft, mariners, and citizens from the intermittent volcanic activity. These notifications led to fairly straightforward actions to ensure that aircraft divert around any ash-bearing cloud or cancel the flight, marine vessels avoid the island, and local residents and mariners take precautions to reduce exposure to ash. No evacuations were necessary due to lack of population proximal to Bogoslof.

Conclusions

The 9-month-long eruption of Bogoslof in 2016–2017 included 70 explosive events and at least two episodes of subaerial dome building. A combination of distant seismic stations, regional infrasound sensors and lightning detection, a variety of satellite data and observer reports, and a field visit in 2018 was used to recreate the events that occurred during the eruption, though the lack of direct observations and local sensors means that much detail was lost. Following precursory seismicity that began in September 2016, the eruption began in December 2016 with a series of explosive events that persisted through mid-March 2017. After a 6-week hiatus, activity resumed on May 17 and lasted through the end of August 2017 and consisted of additional explosions and two short-lived subaerial lava domes that formed in June and August. For most of the eruption, Bogoslof's vent was submerged in shallow seawater, though during several of the longer events a subaerial edifice grew, and the vent migrated above sea level resulting in more ash-rich volcanic clouds. Despite this Surtseyan setting, eruptive products, geophysical signals, and eruptive style are all broadly consistent with vulcanian activity—where slow magma ascent leads to repetitive dome or plug formation, overpressurization in the upper conduit, and sudden release during short-lived explosions. Infiltration of seawater certainly played a role in eruption dynamics, for example, it may have prohibited large domes from forming especially in the first half of the eruption when explosions were closely spaced in time. Because of the lack of direct observations, however, classic Surtseyan behavior may have gone undetected. Impacts from the eruption include three episodes of ashfall on nearby communities and mariners, and dozens of flight cancelations and flight diversions around the volcano and its ash clouds.

Acknowledgments Initial observations and data gathering during the eruption response were performed by a large team at AVO, which is a cooperative program of the US Geological Survey, the Alaska Division of Geological & Geophysical Surveys, and the University of Alaska Fairbanks Geophysical Institute. In particular, we thank Gabrielle Tepp, Matt Haney, and Dave Schneider for providing input that improved the chronology, though responsibility for any remaining inaccuracies remains with the authors. We thank Evan Thoms for assistance with map-based figures. Remote sensing data and observations from the National Civil Applications Center in Reston, Virginia was a valuable resource. The authors thank Sarah Ogburn, an anonymous reviewer, and editor Andy Harris for constructive reviews.

Funding information Funding for this study was provided by the USGS Volcano Hazards Program, including funds provided through USGS Cooperative Agreement No. G19AC00165.

References

Behnke SA, Thomas RJ, McNutt SR, Schneider DJ, Krehbiel PR, Rison W, Edens HE (2013) Observations of volcanic lightning during the 2009 eruption of Redoubt Volcano. J Volcanol Geotherm Res 259: 214–234. https://doi.org/10.1016/j.jvolgeores.2011.12.010

Bohnenstiehl DR, Dziak RP, Matsumoto H, Lau T-KA (2013) Underwater acoustic records from the March 2009 eruption of Hunga Ha'apai-Hunga Tonga volcano in the Kingdom of Tonga. J Volcanol Geotherm Res 249:12–24. https://doi.org/10.1016/j.jvolgeores.2012.08.014

Cheshire, L (2017) Ash cloud restricts Asia-US airfreight. Asia Fruit 27, 2017

Churikova T, Dorendorf F, Worner G (2001) Sources and fluids in the mantle wedge below Kamchatka, evidence from across-arc geochemical variation. J Petrol 42:1567–1593

Clarke AB, Stephens S, Teasdale R, Sparks RSF, Diller K (2007) Petrologic constraints on the decompression history of magma prior to Vulcanian explosions at the Soufrière Hills volcano, Montserrat. J Volcanol Geotherm Res 161:261–274

Coombs ML, Wech A, Haney M, Lyons J, Schneider DJ, Schwaiger H, Wallace K, Fee D, Freymueller J, Schaefer J (2018) Short-term forecasting and detection of explosions during the 2016–2017 eruption of Bogoslof volcano, Alaska. Front Earth Sci 6:122. https://doi.org/10.3389/feart.2018.00122

Druitt TH, Young SR, Baptie BJ, Bonadonna C, Calder ES, Clarke AB, Cole PD, Harford CL, Herd RA, Lockett R, Ryan G, Voight B (2002) Episodes of cyclic Vulcanian explosive activity with fountain collapse at Soufrière Hills Volcano, Montserrat. Geol Soc Lond Mem 21:281–306

Ewert JW, Diefenbach AK, Ramsey DW (2018) 2018 update to the U.S. Geological Survey national volcanic threat assessment. US Geol Sur Sci Invest Report 2018–5140. https://doi.org/10.3133/sir20185140

Fee D, Lyons J, Haney M, Wech A, Waythomas CF, Diefenbach A, Lopez T, Van Eaton AR, Schneider D (2019) Seismo-acoustic evidence for vent drying during shallow submarine eruptions at Bogoslof volcano, Alaska. Bull Volcanol. https://doi.org/10.1007/s00445-019-1326-5

Guffanti M, Casadevall TJ, Budding K (2010) Encounters of aircraft with volcanic ash clouds: a compilation of known incidents, 1953–2009. US Geol Sur Data Series 545

Guffanti M, Miller T (2013) A volcanic activity alert-level system for aviation: review of its development and application in Alaska. Nat Hazards 69:1519–1533. https://doi.org/10.1007/s11069-013-0761-4

Haney MM, Fee D, McKee KF, Lyons JJ, Matoza R, Wech A, Tepp G, Searcy S, Mikesell TD (2019a) Co-eruptive tremor from Bogoslof volcano, Alaska: seismic wavefield composition at regional distances. Bull Volcanol (part of the Bogoslof Topical Collection)

Haney M, Van Eaton AR, Lyons J, Kramer RL, Fee D, Iezzi A, Dziak R, Anderson, Johnson (2019b) Characteristics of volcanic thunder and electromagnetic pulses from lightning at Bogoslof. Bull Volcanol (part of the Bogoslof Topical Collection)

Haney MM, Van Eaton AR, Lyons JJ, Kramer RL, Fee D, Iezzi AM (2018) Volcanic thunder from explosive eruptions at Bogoslof volcano, Alaska. Geophys Res Lett 45:3429–3435. https://doi.org/10.1002/2017GL076911

Houghton B, While J, Van Eaton A (2015) Phreatomagmatic and related eruption styles. In Sigurdsson H (ed) The Encyclopedia of Volcanoes, 2nd Ed. Academic Press, pp 537–552

Horwell CJ, Baxter PJ (2006) The respiratory health hazards of volcanic ash: a review for volcanic risk mitigation. Bull Volcanol 69:1–24

Kokelaar BP (1983) The mechanism of Surtseyan volcanism. J Geol Soc 140:939–944

Loewen M, Izbekov P, Moshrefzadeh J, Graham N, Larsen JF, Coombs ML, Waythomas CF, Wallace K (2019) Petrology of the 2016–2017 eruption of Bogoslof volcano, Alaska. Bull Volcanol (part of the Bogoslof Topical Collection)

Lopez T, Clarisse L, Schwaiger H, Van Eaton AR, Fee D, Carn S, Prata F, Searcy C, Lyons J, Wech A, Haney M, Wallace K (2019) Insights into eruption processes at Bogoslof volcano through evaluation of event SO2 masses and comparison with complementary datasets. Bull Volcanol (part of the Bogoslof Topical Collection)

Lyons J, Haney M, Fee D, Wech A, Waythomas C (2019a) Infrasound from giant bubbles during explosive submarine eruptions of Bogoslof volcano, Alaska. Nat Geosci. https://doi.org/10.1038/s41561-019-0461-0

Lyons J, Iezzi A, Fee D, Schwaiger H, Wech A, Haney M (2019b) Infrasound generated by the 2016–2017 shallow submarine eruption of Bogoslof volcano, Alaska. Bull Volcanol (part of the Bogoslof Topical Collection)

Mastin L, Witter J (2000) The hazards of eruptions through lakes and seawater. J Volcanol Geotherm Res 97:195–214

McGimsey RG, Neal CA, Doukas MP (1995) Volcanic activity in Alaska: summary of events and response of the Alaska Volcano Observatory 1992. US Geol Sur Open File Rep 95–83

McNutt S, Thompson G, West M, Fee D, Stihler S, Clark E (2013) Local seismic and infrasound observations of the 2009 explosive eruptions of Redoubt Volcano, Alaska. J Volcanol Geotherm Res 259:63–76. https://doi.org/10.1016/j.jvolgeores.2013.03.016

Merriam, CH (1901) The birth of an American volcano, Bogoslof in Bering Sea. Everybodys Magazine 5

National Marine Fisheries Service (2017) Fisheries of the United States, 2016. U.S. Department of Commerce, NOAA Current Fishery Statistics No. 2016. Available at: https://www.fisheries.noaa.gov/resource/document/fisheries-united-states-2016-report. Accessed 15 Sept 2019

Neal CA, Brantley SR, Antolik L et al (2018) The 2018 rift eruption and summit collapse of Kīlauea Volcano. Science 363:367–374. https://doi.org/10.1126/science.aav7046

Rutherford MJ, Hill PM (1993) Magma ascent rates from amphibole breakdown; an experimental study applied to the 1980–1986 Mount St. Helens eruptions. J Geophys Res 98:19667–19685

Schneider D, Van Eaton AR, Wallace K (2019) Satellite observations of the 2016–17 eruption of Bogoslof volcano: aviation and ash fallout hazard implications from a water-rich eruption. Bull Volcanol (part of the Bogoslof Topical Collection)

Schwaiger HF, Denlinger RP, Mastin LG (2012) Ash3D: a finite-volume, conservative numerical model for ash transport and tephra deposition. J Geophys Res 117:B04204. https://doi.org/10.1029/2011JB008968

Schwaiger H, Lyons J, Iezzi A, Fee D (2019) Evolving infrasound detections from Bogoslof volcano, Alaska: insights from forward modelling. Bull Volcanol (part of the Bogoslof Topical Collection)

Searcy C, Power J (2019) Seismic durations of explosive events during the 2016–2017 eruption of Bogoslof Volcano, Alaska. Bull Volcanol (part of the Bogoslof Topical Collection)

Sobel Z (2017) Eruptions can't stop sealife from calling Bogoslof home. KUCB 20:2017

Tepp G (2018) A repeating event sequence alarm for monitoring volcanoes. Seism Res Lett 89:1863–1876

Tepp G and Haney M (2019) Short-term explosion precursors during the 2016–2017 Bogoslof eruption. Bull Volcanol (part of the Bogoslof Topical Collection)

Tepp G, Power JA, Dziak R, Searcy C, Lyons J, Haney M, Haxel, Matsumoto (2019) Seismic and hydroacoustic observations of the 2016–17 Bogoslof eruption. Bull Volcanol (part of the Bogoslof Topical Collection)

Van Eaton AR, Schneider DJ, Smith CM, Haney MM, Lyons JJ, Said R, Fee D, Holzworth RH, Mastin LG (2019) Did ice-charging generate

volcanic lightning during the 2016–2017 eruption of Bogoslof volcano, Alaska? Bull Volcanol (part of the Bogoslof Topical Collection)

Vaughan RG, Webley PW (2010) Satellite observations of a surtseyan eruption: Hunga Ha'apai, Tonga. J Volcanol Geotherm Res 198: 177–186

Waythomas CF, Cameron C (2018) Historical eruptions and hazards at Bogoslof volcano, Alaska. US Geol Sur Sci Invest Rep 2018–5085. doi: https://doi.org/10.3133/sir20185085

Waythomas CF, Angeli K, Wessels R, Schneider D. (2019a) 2016-17 evolution of the submarine-subaerial edifice of Bogoslof volcano, Alaska, based on analysis of satellite imagery. Bull Volcanol (part of the Bogoslof Topical Collection)

Waythomas CF, Loewen M, Larsen JF, Wallace K, Cameron C (2019b) Geology and eruptive history of Bogoslof volcano. Bull Volcanol (part of the Bogoslof Topical Collection)

Waythomas CF, Mastin L (2019) Ballistics erupted during the eruption of Bogoslof volcano, Alaska. Bull Volcanol (part of the Bogoslof Topical Collection)

Wech A, Tepp G, Lyons J, Haney M (2018) Using earthquakes, T waves, and infrasound to investigate the eruption of Bogoslof volcano, Alaska. Geophys Res Lett 45:6918–6925. https://doi.org/10.1029/2018GL078457

Wilson TM, Stewart C, Sword-Daniels V, Leonard GS, Johnston DM, Cole JW, Wardman J, Wilson G, Barnard ST (2012) Volcanic ash impacts on critical infrastructure. Phys Chem Earth Parts A/B/C 45: 5–23. https://doi.org/10.1016/j.pce.2011.06.006